JOURNAL OF COMPUTATIONAL PHYSICS 110, 407–418 (1994)

A High Performance Spectral Code for Nonlinear MHD Stability

MARK TAYLOR*

Courant Institute of Mathematical Sciences, 251 Mercer Street, New York, New York 10012

Received September 3, 1992; revised August 2, 1993

A new spectral code, NSTAB, has been developed to do nonlinear stability and equilibrium calculations for the magnetohydrodynamic (MHD) equations in three-dimensional toroidal geometries. The code has the resolution to test nonlinear stability by calculating bifurcated equilibria directly. These equilibria consist of weak solutions with current sheets near rational surfaces and other less localized modes. Bifurcated equilibria with a pronounced current sheet where the rotational transform crosses unity are calculated for the international thermonuclear experimental reactor (ITER). Bifurcated solutions with broader resonances are found for a model of the LHD stellarator currently being built in Japan and an optimized configuration like the Wendelstein VII-X proposed for construction in Germany. The code is able to handle the many harmonics required to capture the high mode number of these instabilities. NSTAB builds on the highly successful BETAS code, which applies the spectral method to a flux coordinate formulation of the variational principle associated with the MHD equilibrium equations. A new residue condition for the location of the magnetic axis has been developed and implemented. This condition is based on the weak formulation of the equations and imposes no constraints on the inner flux surfaces.

1. INTRODUCTION

The magnetohydrodynamic (MHD) equations describe the macroscopic behavior of a plasma in a magnetic field. They have been used successfully to model many aspects of tokamaks and stellarators. The finite difference code BETA [1, 2] implemented one of the first numerical methods to solve the time averaged ideal MHD equilibrium equations in three-dimensional toroidal geometries. It has been used extensively for designing stellarators, performing parameter studies, and studying nonlinear stability and Monte Carlo transport in both stellarators and tokamaks [3–6]. More accurate results have been made possible by the development of the spectral codes VMEC [7, 8] and BETAS [9]. These codes use Fourier series expansions in the two periodic angles on the torus and finite differences in the radial direction. VMEC was one of the first successful spectral codes, and is the most widely used today. The BETAS code improved the speed of the computational method with the development of a preconditioned second-order iterative scheme. This feature has since been incorporated into VMEC [10].

This paper describes a new equilibrium code, NSTAB, and demonstrates how it is used to test nonlinear stability. NSTAB contains a new residue condition for the location of the magnetic axis, developed from the variational principle and the concept of a weak solution. The resultant axis equations are substantially different from those used by BETAS and VMEC, which are based on linear extrapolation and impose constraints on the innermost flux surface. The residue condition requires no such contraints, so for complicated geometries it allows for more realistic shapes at standard meshes and may provide a more accurate value for the energy. Other aspects of the code are based largely on BETAS.

Several codes have been developed to study stability properties of MHD equilibria. Methods based on normal mode analysis are used in [11, 12]. Equibrium codes have also been used for stability calculations by performing first an energy minimization to arrive at an equilibrium solution and then a second constrained energy minimization to look for regions in function space with lower energy levels [2]. Both NSTAB and BETAS have the resolution to perform a more direct kind of stability test. Due to the coordinate system, the arrangement of the unkowns, and the radial differencing scheme, these codes can capture weak solutions with current sheets near rational surfaces and other less localized modes that are important in the applications. This allows one to test for nonlinear instability by looking for bifurcated solutions that demonstrate strong nonuniqueness. Results along these lines will be presented for several configurations of interest.

Energy level comparisons by the spectral method turn out to be difficult. The bifurcated solutions may have lower energy levels when compared to a more standard equilibrium solution on the same mesh, but the difference is very small. A true convergence study, with extrapolation to zero mesh size, would have to be performed before the energy

* Present address: National Center for Atmospheric Research, P.O. Box 3000, Boulder, CO 80307-3000. email: taylorm@ncar.ucar.edu.

0021-9991/94 $6.00

comparisons can be considered meaningful. Configurations like the axisymmetric tokamak or one field period of the LHD stellarator do not have complicated structure and accurate solutions can be computed quickly at crude meshes. In contrast, the weak solutions characterizing unstable modes tend to have much higher harmonics and represent a true challenge to the code. It is thus impractical to perform the extrapolation to zero mesh size required for true energy level comparisons in all these cases, but the existence of the bifurcated solutions themselves can be determined by relatively short runs, and this forms the basis of our nonlinear stability test.

An improved flux coordinate formulation of the variational principle which clarifies the role of weak solutions and the nested surface hypothesis is outlined in Section 2 of this paper. Problems with the coordinate system at the magnetic axis and the derivation of a new axis residue condition are described in Section 3. Details of the numerical implementation of these ideas are contained in Section 4, and numerical results are presented in Sections 5 through 8. Finally, Section 9 consists of concluding remarks.

2. MATHEMATICAL MODEL

To determine the structure of the magnetic field in the plasma we use the magnetohydrodynamic equilibrium equations

$$\nabla \cdot \mathbf{B} = 0, \tag{1}$$

$$\mathbf{J} \times \mathbf{B} = \nabla p, \tag{2}$$

where $\mathbf{B}$ is the magnetic field, p is the scalar pressure, and $\mathbf{J}$ is the current density defined by $\mathbf{J} = \nabla \times \mathbf{B}$.

These equations are to be solved in three-dimensional toroidal domains. Following earlier work [1], several assumptions are imposed to make the problem computationally tractable. We assume the existence of a nested family of toroidal flux surfaces of $\mathbf{B}$, labeled by s. We take $s = 1$ to represent the plasma boundary and $s = 0$ to represent the innermost degenerate flux surface, which is a simple closed curve called the magnetic axis. On each torus $s = \text{const.}$ we introduce periodic coordinates u and v, representing the poloidal and toroidal angles, respectively. We define the net toroidal flux in a solid torus $s < s_0$ to be the flux of $\mathbf{B}$ through a cross section $v = \text{const}$. This is independent of which cross section is used because $\nabla \cdot \mathbf{B} = 0$. In most cases of interest $\mathbf{B}$ will have a strong toroidal component that does not reverse direction, so we further assume that we can choose s itself to be the normalized toroidal flux.

We can now integrate the equation $\nabla \cdot \mathbf{B} = 0$ by setting

$$\mathbf{B} = \nabla s \times \nabla \theta,$$

where the level sets $\theta = \text{const}$ define another set of flux surfaces. Locally, every divergence-free vector field has such a representation, but in general s and θ will not have single-valued global extensions. Under the nested surface hypothesis s is single-valued, and θ must have the form

$$\theta = u - \iota(s)v + \tilde{\theta}(s, u, v),$$

where $\tilde{\theta}$ is periodic in u and v. Here the rotational transform $\iota(s)$ is the derivative of the poloidal flux with respect to s.

Returning to the force balance equation (2) and taking a dot product with $\mathbf{B}$, we see that $\mathbf{B} \cdot \nabla p = 0$, which means that p is constant on magnetic field lines. In our formulation of the variational principle this magnetic differential equation has been integrated by putting $p = p(s)$. We are thus left with two equations in two unknowns, s and θ. There are no boundary conditions on θ other than the periodicity requirements mentioned above, but θ is only determined up to an arbitrary function of s.

There are two arbitrary functions $p(s)$ and $\iota(s)$ in the model. The pressure $p(s)$ will be prescribed, although physically it would be more natural to give the mass within each flux tube $s = \text{const}$ and to compute $p(s)$ from the equation of state. This simplification seems to produce more or less equivalent results about equilibrium and stability. The treatment of the rotational transform depends on the type of experiment we are modeling. In a tokamak, $\iota(s)$ is prescribed, which fixes the net poloidal flux as a function of the net toroidal flux. For stellarators this constraint is dropped and $\iota(s)$ is treated as one of the unknowns. Its value is determined by minimizing the energy, which is achieved at zero net toroidal current.

The considerations we have just described are contained in the standard variational principle of magnetohydrodynamics. The energy of the plasma, defined by

$$\mathbf{E} = \iiint \left(\tfrac{1}{2}B^2 - p(s)\right) dV, \tag{3}$$

is minimized subject to the following constraints:

1. There is a nested family of toroidal flux surfaces. Each surface is labeled by s, the normalized toroidal flux that it encloses.
2. In a tokamak, $\iota(s)$ is prescribed. For stellarators, this constraint is dropped and $\iota(s)$ is chosen to minimize the energy, which is achieved at zero net toroidal current.
3. The pressure $p(s)$ is prescribed.
4. The location of the plasma boundary $s = 1$ is given.

The Euler–Lagrange equations in the calculus of variations, which come from formally minimizing the energy for all possible functions s and θ subject to these constraints, are equivalent to the MHD equilibrium equation (2). Equation

(1) is imposed as a flux constraint by the use of s and θ in the representation of **B**.

For several important reasons our computations will be performed with s, u, and v as the independent variables. This gives a convenient rectangular computational domain and allows us to implement the flux constraints $p = p(s)$ and $\iota = \iota(s)$. It also permits us to define θ uniquely.

The restriction to nested flux surface configurations greatly simplifies the model, but there are theoretical issues concerning the validity of this assumption. There are axisymmetric solutions in special cases which do satisfy the nested surface hypothesis, but the KAM theorem has been used to demonstrate the nonexistence of smooth equilibria in three dimensions. Line-tracing codes which track magnetic field lines in a vacuum show that islands can appear at rational surfaces. The islands consist of smaller tori which can themselves be nested. Even in axisymmetric cases where solutions with nested surfaces do exist, there are resonances at rational surfaces where significant instabilities can be found by introducing three-dimensional perturbations.

The NSTAB code handles these problems within the framework of the nested flux surface topology by calculating weak solutions [3]. The weak solutions can include current sheets which develop at rational surfaces and serve to model magnetic islands. Numerical examples of these weak solutions are presented in Section 6. A current sheet represents a jump in the tangential components of **B** resulting in a surface current and is analogous to the widely accepted vortex sheet model of fluid dynamics. In our calculations it appears as an intersection of two or more flux surfaces. The variational principle is used to define the concept of a weak solution, which suggests how to capture such solutions numerically by giving a natural conservation form of the MHD equations.

We now derive the MHD equations in the s, u, v coordinate system. Let x_1, x_2, and x_3 be the usual Cartesian coordinates and introduce cylindrical coordinates $A + r$, z, and v, where A is the major radius of the confinement device, and

$$x_1 = (A + r)\cos(2\pi v), \qquad x_2 = (A + r)\sin(2\pi v), \qquad x_3 = z.$$

The choice of the poloidal angle u is arbitrary and will be determined by how the shape of the outer plasma wall is parametrized. We take $r_1 = r_1(u, v)$ and $z_1(u, v)$ to be a given parametrization of the outer wall $s = 1$, and we let $r_0(v)$ and $z_0(v)$ represent the location of the magnetic axis $s = 0$. Imposing a star-like condition on the shape of the flux surfaces, we write

$$r = r_0(v) + R(s, u, v)[r_1(u, v) - r_0(v)],$$
$$z = z_0(v) + R(s, u, v)[z_1(u, v) - z_0(v)],$$

where R is a generalized radius that is zero at $s = 0$ and 1 at $s = 1$. Computations will be carried out to solve for the unknowns θ, R, r_0, and z_0 as functions of s, u, and v. To derive equations for these quantities, the energy integral E is written in this coordinate system and the Euler–Lagrange equations are calculated.

The Jacobian of the transformation $(s, u, v) \to (x_1, x_2, x_3)$ has the remarkable factorization

$$\frac{\partial(x_1, x_2, x_3)}{\partial(s, v, u)} = K\frac{\partial(r, z)}{\partial(s, u)} = KHRR_s, \tag{4}$$

where

$$H = \frac{\partial z_1}{\partial u}(r_1 - r_0) - \frac{\partial r_1}{\partial u}(z_1 - z_0)$$

depends only on u and v and $K = 2\pi(A + r)$ is the Jacobian from Cartesian to cylindrical coordinates. The evaluation of the Jacobian is crucial if the numerical method is to capture weak solutions where it becomes singular. Separation of the Jacobian into an angle factor H independent of s and the radial factor RR_s, involving just one derivative, seems to account for the high accuracy in the computations. In the radial direction where discontinuities occur, the s derivative is isolated to the term RR_s which can be computed with very little truncation error. We believe it is the combination of this factorization of the Jacobian and the radial differencing scheme that allows weak solutions to be captured effectively.

To write **B** in this coordinate system, we exploit the invariance of Jacobians to observe that

$$\mathbf{B} = \mathbf{B}\cdot\nabla\mathbf{X} = (\nabla s \times \nabla\theta)\cdot\nabla\mathbf{X}$$
$$= \frac{\partial(s, \theta, \mathbf{X})}{\partial(x_1, x_2, x_3)} = \frac{\theta_u\mathbf{X}_v - \theta_v\mathbf{X}_u}{KHRR_s},$$

where **X** is the position vector. Now the energy integral (3) can be written in the elegant form

$$\mathbf{E} = \iiint \left(\frac{(\theta_u\mathbf{X}_v - \theta_v\mathbf{X}_u)^2}{2KHRR_s} - p(s)\,KHRR_s\right) ds\,du\,dv.$$

We proceed to derive a weak form of the Euler–Lagrange equations from the general expression for the first variation of the energy with respect to an arbitrary displacement in the unknowns

$$\delta E = \iiint [\mathbf{B}\cdot\delta(\theta_u\mathbf{X}_v - \theta_v\mathbf{X}_u) - (\tfrac{1}{2}B^2 + p)\,\delta(KHRR_s)] \times ds\,du\,dv. \tag{5}$$

To compute the first variation with respect to $\delta\theta$, we put

$\delta(\theta_u \mathbf{X}_v - \theta_v \mathbf{X}_u) = \mathbf{X}_v\,\delta\theta_u - \mathbf{X}_u\,\delta\theta_v$ and note that $KHRR_s$ does not depend on θ. Using Eq. (5) we obtain

$$\delta E_1 = \iiint [(\mathbf{B}\cdot\mathbf{X}_v)\,\delta\theta_u - (\mathbf{B}\cdot\mathbf{X}_u)\,\delta\theta_v]\,ds\,du\,dv. \quad (6)$$

To derive the first variation with respect to R, we use the identity $\delta(KHRR_s) = (KHR\,\delta R)_s$ and find

$$\delta E_2 = \iiint [\theta_u \mathbf{B}\cdot(\mathbf{X}_R\,\delta R)_v - \theta_v \mathbf{B}\cdot(\mathbf{X}_R\,\delta R)_u - (\tfrac{1}{2}B^2 + p)(KHR\,\delta R)_s]\,ds\,du\,dv. \quad (7)$$

Since no second-order derivatives appear in Eq. (6) and (7), we need only assume that the unknowns R and θ have first derivatives. A weak solution is thus defined as a pair of functions R and θ that satisfy the integral equations $\delta E_1 = 0$ and $\delta E_2 = 0$ for all continuously differentiable test functions $\delta\theta$ and δR.

Returning to (6), we integrate twice by parts and obtain the Euler–Lagrange equation

$$L_1(\theta) = (\mathbf{B}\cdot\mathbf{X}_v)_u - (\mathbf{B}\cdot\mathbf{X}_u)_v = 0.$$

This equation is left in the conservation form that results from the variational principle. From Eq. (7), we can similarly derive the pseudo-conservation form (undifferentiated terms also appear) of the Euler–Lagrange equation $L_2(R) = 0$. However, a slight rearrangement of the terms leads to the computationally more efficient formula

$$L_2(R) = \frac{1}{R_s}\{\theta_v[(\mathbf{B}\cdot\mathbf{X}_u)_s - (\mathbf{B}\cdot\mathbf{X}_s)_u] + \theta_u[(\mathbf{B}\cdot\mathbf{X}_s)_v - (\mathbf{B}\cdot\mathbf{X}_v)_s] - p'(s)\,KHRR_s\}.$$

In the case of a stellarator, where the rotational transform $\iota(s)$ is not held fixed, it must be determined by minimizing the energy. The first variation of the energy with respect to ι is

$$\delta E = \iiint (\mathbf{B}\cdot\mathbf{X}_u)\,\delta\iota(s)\,ds\,du\,dv = \int I(s)\,\delta\iota(s)\,ds,$$

where

$$I(s_0) = \iint \mathbf{B}\cdot\mathbf{X}_u\,du\,dv$$

is the net toroidal current through the region enclosed by the flux surface $s = s_0$. Thus the Euler–Lagrange equation which determines $\iota(s)$ is the zero net current condition $I(s) = 0$.

3. AXIS RESIDUE CONDITION

The two Euler–Lagrange equations $L_1(\theta) = 0$ and $L_2(R) = 0$, the pressure constraint $p = p(s)$ and the representation $\mathbf{B} = \nabla s \times \nabla\theta$ are equivalent to the magnetostatic equations (1) and (2). However, we must still derive equations for r_0 and z_0, which determine the location of the magnetic axis. Because of our use of a polar coordinate system there is a singularity at the magnetic axis $s = 0$ and we need equations to guarantee that the solution will remain continuous there. By allowing for this singularity, we have developed a new regularity condition that comes from a more careful consideration of weak solutions defined by the variational method.

If we repeat the procedure used to derive the equations $L_1 = 0$ and $L_2 = 0$, two additional Euler–Lagrange equations can be found by calculating the first variation of the energy with respect to the axis location r_0 and z_0. These equations have been implemented in previous codes with mixed success. Apparently numerical errors involved in many of the terms can become larger than the more critical quantities.

The VMEC and BETAS spectral codes have relied on the Taylor series expansion of s near the magnetic axis to generate equations and constraints on the innermost flux surfaces. This expansion suggests that when the flux surfaces contract down to the magnetic axis, the limiting shape has an elliptical cross section. In BETAS, the innermost surface is required to have elliptical cross sections. The equations for the axis location and the parameters describing the ellipses are derived from the variational principle. In VMEC the axis location is computed by linear extrapolation from the location of the first and second flux surfaces. Higher Fourier coefficients which describe non-elliptical shapes of the innermost flux surface are determined from their values on the second flux surface in a way that is consistent with the Taylor expansion of s.

The regularity condition implemented by NSTAB comes, instead, directly from the variational principle and requires no constraints on the innermost flux surface. We use the fact that there is a singularity at the axis to isolate the most critical quantities. Since the unknowns r_0 and z_0 are functions of v alone, we are free to integrate the terms in the first variation of the energy by parts with respect to s and u. When this is done in a natural way the resulting equations turn out to involve simple combinations of $L_1(\theta)$ and $L_2(R)$. However, there is a residue at $s = 0$ so integration by parts in s can only be carried out away from the magnetic axis. When this integration by parts is performed outside a small flux tube $s = s_0$ containing the axis, a residual surface integral at $s = s_0$ remains, forming the basis of our new axis condition.

To derive the residue condition we return to the general form of the first variation of the energy (5) and write

$$\delta(\theta_u \mathbf{X}_v - \theta_v \mathbf{X}_u) = \theta_u \delta\mathbf{X}_v - \theta_v\,\delta\mathbf{X}_v,$$

$$\delta(KHRR_s) = 2\pi HRR_s\,\delta r + K\delta(r_s z_u - r_u z_s),$$

where the vector $\delta\mathbf{X} = \delta r\,\hat{\mathbf{r}}(v) + \delta z\,\hat{\mathbf{z}}$ is defined in terms of

unit vectors $\hat{\mathbf{r}}(v)$ and $\hat{\mathbf{z}}$. Here we have used Eq. (4) to write $HRR_s = \partial(r, z)/\partial(s, u)$. The first variation of the energy with respect to r and z is given by

$$\delta E = \iiint [\theta_u \mathbf{B}\cdot\delta\mathbf{X}_v - \theta_v \mathbf{B}\cdot\delta\mathbf{X}_u - (\tfrac{1}{2}B^2 + p)\, 2\pi HRR_s\, \delta r - (\tfrac{1}{2}B^2 + p)\, K\delta(r_s z_u - r_u z_s)\, ds\, du\, dv = \iiint T\, ds\, du\, dv,$$

where the symbol T is used to denote the integrand. To compute the first variation with respect to the axis location r_0 and z_0, we first integrate by parts to remove all derivations from δr and δz. We then use $r = r_0 + R(r_1 - r_0)$ and the similar relation for z to obtain

$$\delta r = (1 - R)\, \delta r_0, \qquad \delta z = (1 - R)\, \delta z_0.$$

Since integration by parts with respect to s can only be done outside an inner flux tube $s = s_0$ containing the magnetic axis, we obtain both a volume term and surface integrals at $s = s_0$ and $s = 1$. The surface integral at $s = 1$ disappears because there $R = 1$.

After performing these steps, the first variation of the energy can be written in the form

$$\delta E = -\iiint_{s>s_0} [L_3'(r)\, \delta r + L_4'(z)\, \delta z]\, ds\, du\, dv + \iiint_{s<s_0} T\, ds\, du\, dv - \iint_{s=s_0} (\tfrac{1}{2}B^2 + p)\, K(r_u\, \delta z - z_u\, \delta r)\, du\, dv.$$

It is easy to verify that

$$r_u L_3'(r) + z_u L_4'(z) = -\theta_u L_1(\theta) = 0,$$
$$(r_1 - r_0)\, L_3'(r) + (z_1 - z_0)\, L_4'(z) = L_2(R) = 0,$$

and by combining these two relations we see that $L_3'(r) = L_4'(z) = 0$ is a consequence of the Euler–Lagrange equations $L_1 = L_2 = 0$. We are therefore left with the residue

$$\delta E = -\iint_{s=s_0} (\tfrac{1}{2}B^2 + p)\, K(1 - R) \times [r_u\, \delta z_0(v) - z_u\, \delta r_0(v)]\, du\, dv + \iiint_{s<s_0} T\, ds\, du\, dv. \tag{8}$$

There are several problems with implementing Eq. (8) numerically. Large terms in the integrand which do not depend on u contribute nothing to the residue, but have numerical errors that dominate the more critical terms. There are also errors arising from quantities in the expression for B^2 which are poorly computed near the magnetic axis. To handle these difficulties we make several simplifications in the integrand.

The first simplification is to keep only the surface integral from Eq. (8) and to neglect the lower order volume term over the region $s < s_0$. The Euler–Lagrange equations then reduce to contour integrals around a closed curve circling the magnetic axis and lying on an arbitrary small inner tube $s = s_0$. Numerically we evaluate this integral over the innermost surface provided by the computational mesh. We may remove terms which do not depend on u, such as $p(s)$, since they will integrate to zero on the closed contour and contribute nothing to the residue. We also divide out the terms $1 - R$ and K because near the magnetic axis they are constant in u to lowest order in s.

The only quantity left is B^2, which can be written in the form

$$B^2 = \frac{(\mathbf{B}\cdot\mathbf{X}_v)^2}{\mathbf{X}_v^2} + \frac{\theta_v^2}{\mathbf{X}_v^2}\frac{|\mathbf{X}_u \times \mathbf{X}_v|^2}{(KHRR_s)^2}.$$

The first term is the norm of the toroidal component of $\mathbf{B}$ and the second term is the norm of the poloidal component. For tokamaks and stellarators, the toroidal magnetic field is much stronger that the poloidal field and the equation $L_1(\theta) = 0$ can be used to show that it is independent of u at the magnetic axis. On the infinitesimal surface $s = s_0$ the toroidal part of B^2 will be nearly constant in u and contribute little to the residue. It is thus preferable to neglect this term, since numerical errors in its calculation may suppress the remaining poloidal part of B^2.

We make a final simplification by replacing $\theta_v^2/\mathbf{X}_v^2$ by a constant. In the axisymmetric case $\theta_v = -\iota(s)$, so this assumption can be justified for configurations close to having such symmetry near the magnetic axis. A similar argument can be made for configurations close to helical symmetry near the axis due to the invariance of the representation of the integrand.

Combining these considerations, the simplified Euler–Lagrange equations are

$$L_3(r_0) = -\int_{s=s_0} \frac{|\mathbf{X}_u \times \mathbf{X}_v|^2}{(KHRR_s)^2}\, z_u\, du = 0,$$

$$L_4(z_0) = \int_{s=s_0} \frac{|\mathbf{X}_u \times \mathbf{X}_v|^2}{(KHRR_s)^2}\, r_u\, du = 0.$$

The most important feature of the equations is the fact that the Jacobian $KHRR_s$ appears in the denominator. This keeps the magnetic axis roughly centered inside the inner-

most flux surface and results in a continuous solution at the axis. For if the axis gets too close to the flux surface $s = s_0$, the Jacobian will become very small and the residue will differ from zero. Another important feature of the equations is that their implementation requires no constraints on the innermost flux surface $s = s_0$. The assumptions made in their derivation do indirectly influence the flux surfaces, but only through the coupling of the axis equations and the Euler–Lagrange equations for R and θ.

To further justify the simplified axis equations we use the identity

$$(\nabla s)^2 = \frac{(Kr_u)^2 + (Kz_u)^2 + (r_u z_v - r_v z_u)^2}{(KHRR_s)^2} = \frac{|\mathbf{X}_u \times \mathbf{X}_v|^2}{(KHRR_s)^2}$$

to write them in the purely geometrical form

$$L_3(r_0) = -\oint_{s=s_0} (\nabla s)^2 \, dz, \qquad L_4(z_0) = \oint_{s=s_0} (\nabla s)^2 \, dr.$$

If we now assume that the innermost flux surface $s = s_0$ has elliptical cross sections $r = a_1 \cos(u)$, $z = a_2 \sin(u)$ with the axis at the center, then the two equations $L_3 = L_4 = 0$ follow to lowest order by Fourier analysis, since $(\nabla s)^2$ behaves like a combination of 1, $\cos(2u)$, and $\sin(2u)$. In this sense, our axis consition is equivalent to the more geometrical considerations used in BETAS. Indeed, in Section 5 we describe the very good agreement between the NSTAB and BETAS codes achieved in several special cases.

4. THE NSTAB COMPUTER CODE

The NSTAB code uses a preconditioned iterative scheme to solve the Euler–Lagrange equations

$$L_1(\theta) = 0, \qquad L_2(R) = 0, \qquad L_3(r_0) = 0, \qquad L_4(z_0) = 0.$$

The scheme is based on the second-order Richardson method invented by Frankel [13], with a preconditioner and an adaptive algorithm used for determining the acceleration parameters due to Betancourt [9]. The combination of the preconditioner and the iterative scheme results in a dramatic improvement in performance as compared to previous schemes [10, 14].

The iteration is performed on the Fourier coefficients of the unknowns R, θ, r_0, and z_0. A combination of the pseudospectral method [15] in the angles on the torus and a finite difference scheme in the radial direction is used. At each step in the iteration, the variables R, θ, r_0, z_0 and their u and v derivatives are first computed at equally spaced collocation points in u and v from their Fourier coefficients. Finite differences and a staggered grid described in [2, 3] are used to compute the s derivatives. The terms in the operators $L_1(\theta)$, $L_2(R)$, $L_3(r_0)$, and $L_4(z_0)$ are then evaluated at the collocation points. Finally their Fourier coefficients are computed and used by the iterative scheme to compute new values for the Fourier coefficients of the unknowns. Further details may be found in [14].

The differencing scheme provides high resolution and minimal coupling between flux surfaces when combined with our simple representation for the Jacobian $KHRR_s$. These properties are desirable if current sheets and other localized modes are to be captured accurately. The difference formulas are chosen to be second-order accurate and to give the exact answer in the example of a one-dimensional screw pinch. Codes based on similar and more elaborate differencing schemes [8], but with a different arrangement of the unknowns, do not seem to have the resolution to calculate solutions with current sheets and other types of modes as accurately as NSTAB and BETAS.

The NSTAB code takes as input the parametrization in u and v of the separatrix which defines the outer plasma wall. The coordinate v has been defined as the toroidal angle, but the definition of u is arbitrary. The actual location on a flux surface of the equally spaced mesh points in u will depend on how the outer wall is parametrized and on the location of the magnetic axis.

Let ϕ represent the polar angle in the coordinate system centered at the magnetic axis. The coordinate system puts the mesh points at the intersection of the rays $\phi = \text{const}$ and the flux surfaces $s = \text{const}$. If the outer wall is far from circular, or if the magnetic axis is substantially shifted from the center of the plasma, points equally spaced in arc length along the boundary will not necessarily be equally spaced in ϕ, and that results in poor spacing on the flux surfaces near the magnetic axis. In practice, we rezone the parametrization of the outer wall to obtain a compromise between equally spaced points in arc length on the boundary versus equally spaced points in ϕ. This simple method works well but does require some care. A more sophisticated procedure, where the zoning is chosen to maximize the convergence of the Fourier series of the other unknowns, is described in [16]. However, that method is questionable because it introduces an additional unknown.

The coordinates of the outer wall r_1 and z_1 are defined by

$$r_1 + iz_1 = e^{iu} \sum_{m,n} \Delta_{m,n} e^{-i(mu - nv)}.$$

We have used this formula because it provides a natural association between the coefficients $\Delta_{m,n}$ and the corresponding harmonics in the winding law used to determine the separatrix. Zoning is handled by making the change of variable

$$u = u' + \sum_{m,n} Z_{m,n} \sin(mu' - nv),$$

with collocation points chosen to be equally spaced in u'. In the simplest cases only $Z_{1,0}$ is nonzero, to account for an outward shift in the position of the magnetic axis. In harder examples such as the H1 Heliac, where the outer wall is far from circular, proper zoning is critical for good convergence. It is found that large coefficients $\Delta_{m,n}$ may require rezoning by the corresponding coefficient $Z_{m,n}$, as can be seen from the calculation of the H1 Heliac in Section 8.

5. CONVERGENCE STUDIES

We now present several studies to demonstrate the convergence properties of the computational method and validate our simplified axis equations. The equilibria used in this study are an axisymmetric tokamak, a straight helical stellarator, and the LHD stellarator being built at the National Institute for Fusion Science in Japan. These cases show that the convergence of the method is only first order with respect to the radial mesh size. In spite of this, the method is still very accurate so that stability tests can be performed with as few as 15 radial points. The well-known high order convergence of the spectral method in the poloidal and toroidal directions is established, and there is very little improvement once one increases the number of harmonics above a certain value. Unfortunately, even in relatively simple cases this threshold is surprisingly high. In terms of the degrees N_u and N_v of the trigonometric polynomials used to represent the solution in the poloidal and toroidal angles, $N_u = N_v = 8$ is adequate for equilibrium, while $N_u = N_v = 16$ may be required for stability.

The axisymmetric tokamak and straight helical equilibria were used to establish the validity of the new axis condition. For these cases we compared NSTAB to BETAS, which has been shown elsewhere to converge to exact solutions [9]. Satisfactory agreement was obtained for the energy levels, since the values computed by NSTAB and BETAS agree to seven figures when extrapolated to zero mesh size. For the axis location the extrapolated values agree to 10^{-4} in units of the plasma radius. These studies also show that the convergence of both the energy and axis location is only first order in the radial mesh size. For complete details, see [14].

The convergence of the energy and axis location with regard to the degrees of the poloidal and toroidal harmonics N_u and N_v are displayed for the LHD stellarator in Figs. 1 and 2. For this study we used an aspect ratio of 6.23 and a pressure profile of $p(s) = 0.41(1 - s)$. This results in a β of 3%, where β is given by

$$\beta = \frac{2 \iiint p \, dV}{\iiint B^2 \, dV}.$$

In each of the 10 field periods, the plasma column forms a rotating ellipse given by $\Delta_{0,0} = 1$ and $\Delta_{2,1} = -0.325$ (see Section 4 for the definition of $\Delta_{m,n}$). The equilibrium calculations were performed over just one field period of the device with 15, 22, 29, and 57 radial points. Clearly $N_u = N_v = 4$ is inadequate, even in this simple case where the plasma column has elliptical cross sections. However, the spectral method has converged quite well as soon as $N_u = N_v = 8$. The figures show that the convergence of the energy and the shift in the magnetic axis is again only first

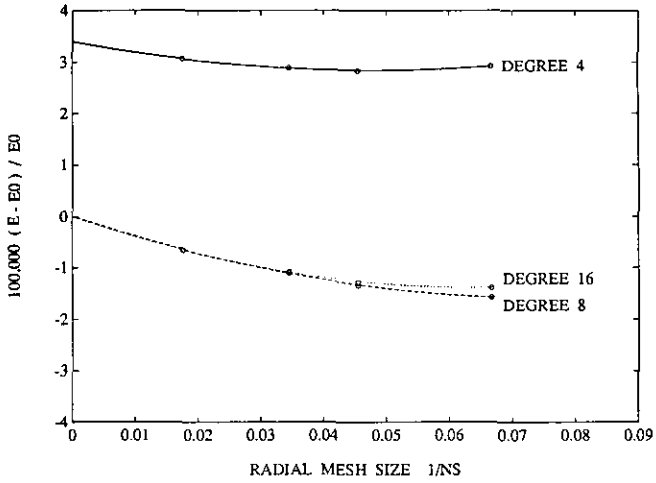

FIG. 1. First-order convergence of the energy E with respect to radial mesh size is shown for the $\beta = 3\%$ LHD stellarator at three degrees of the trigonometric polynomials specifying the spectral truncation. The limited accuracy of the spectral method when $N = 4$ is perhaps surprising for this simple problem where the outer wall is defined by a rotating ellipse. In this case only six figures in the energy are significant and this is too few to resolve stability issues from the energy landscape.

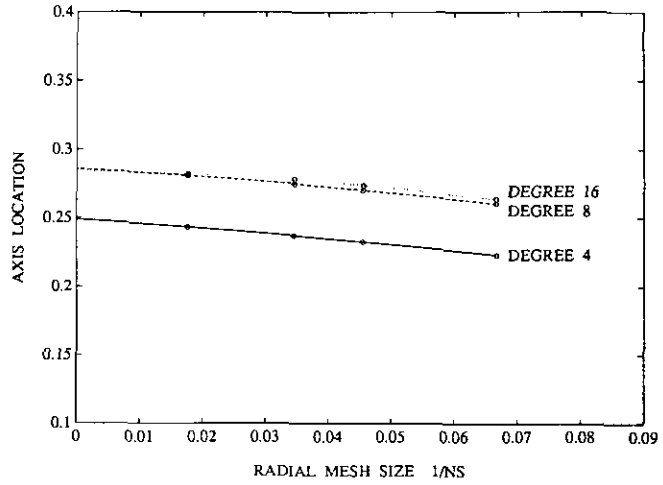

FIG. 2. First-order convergence of the shift in the magnetic axis with radial mesh size is shown for the $\beta = 3\%$ LHD stellarator at different degrees of the trigonometric polynomials specifying the spectral truncation. For a degree N truncation, $4N^2$ terms are used in the spectral representation of the solution and the mesh sizes in the poloidal and toroidal directions are $1/(3N)$.

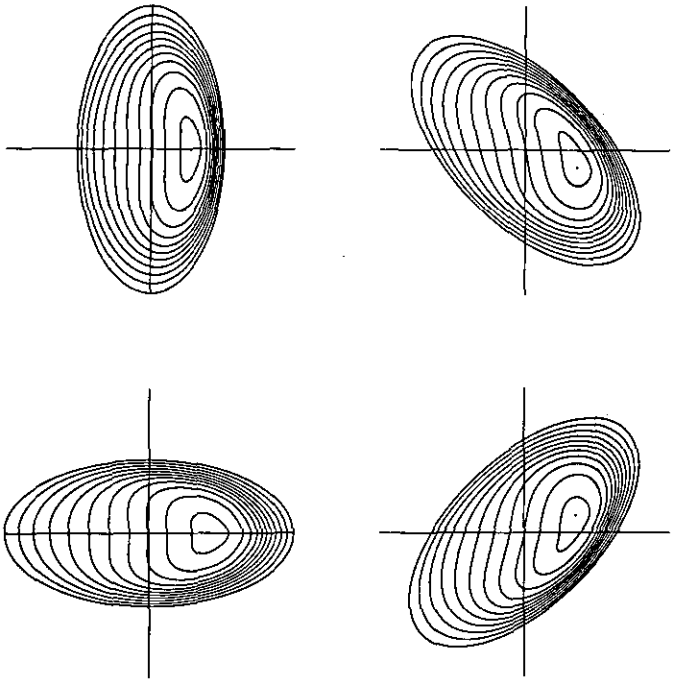

FIG. 3. Flux surfaces in four cross sections of one field period of the LHD stellarator showing the deformed structure of the inner surfaces with an average $\beta = 6\%$. This calculation was performed with 31 radial points and degree eight trigonometric polynomials.

order with respect to the radial mesh size, but that the method is still very accurate. Even at the crudest radial mesh of 15 points, the error in the axis position is only 2% of the plasma radius, which should not affect stability results.

To show the advantages of the new axis condition we compare NSTAB and BETAS in the case of the LHD stellarator with $\beta = 6\%$. At this value of β, the axis has a noticeable helical excursion and a large outward shift which substantially deforms the inner flux surfaces. The results from NSTAB are displayed in Fig. 3. The new axis condition imposes no constraints on the inner flux surfaces, and the calculations show that even at a fine radial mesh these surfaces have a pronounced tear-drop shape. The magnetic axis has an outward shift of 0.48, or half the plasma radius. The BETAS code requires that the innermost flux surface be an ellipse. This in turn forces other surfaces to have less of a tear drop shape and introduces errors over a significant volume of the plasma. The overall effect is that all the flux surfaces become less deformed and the magnetic axis has an outward shift of only 0.36. This is a significant difference because errors in the axis location of this size can affect stability results. At $\beta = 9\%$, NSTAB places the axis at 0.60, resulting in severely deformed flux surfaces which are perhaps incompatible with the imposed elliptical outer wall.

6. CAPTURING CURRENT SHEETS

In this section we demonstrate the high accuracy of the flux coordinate method and its ability to calculate weak solutions with well-resolved current sheets. The success of the method suggests that it could also be used to capture vortex sheets in fluid dynamics. In Fig. 4 a bifurcated equilibrium, calculated with only 12 radial points, is shown for the ITER tokamak [17]. A current sheet has developed so that several flux surfaces intersect at $\iota = 1$. The solution is not axisymmetric, thus by rotating it in the toroidal direction within the axisymmetric torus we can generate a family of equilibria, all identical except for a phase angle in v.

To model the ITER tokamak in these computations, we used an aspect ratio of 3.33, a D-shaped plasma boundary given by $\Delta_{0,0} = 1$, $\Delta_{2,0} = -0.2$, and $\Delta_{-1,0} = 0.2$, and the rotational transform $\iota(s) = 1.2 - 0.75s$. The pressure profile was taken to be $p(s) = 0.04(1 - s)$ with $\beta = 4.4\%$, but the instability is current driven and can be seen even at zero β. The computations were performed with 12 radial, poloidal, and toroidal points with degrees $N_u = N_v = 4$.

The existence of bifurcated equilibria form the basis of our stability test. They confirm the well-known result that a tokamak equilibrium becomes unstable when the rotational transform crosses unity in the plasma. At the meshes we use to make these runs, it is not always practical to rely on the

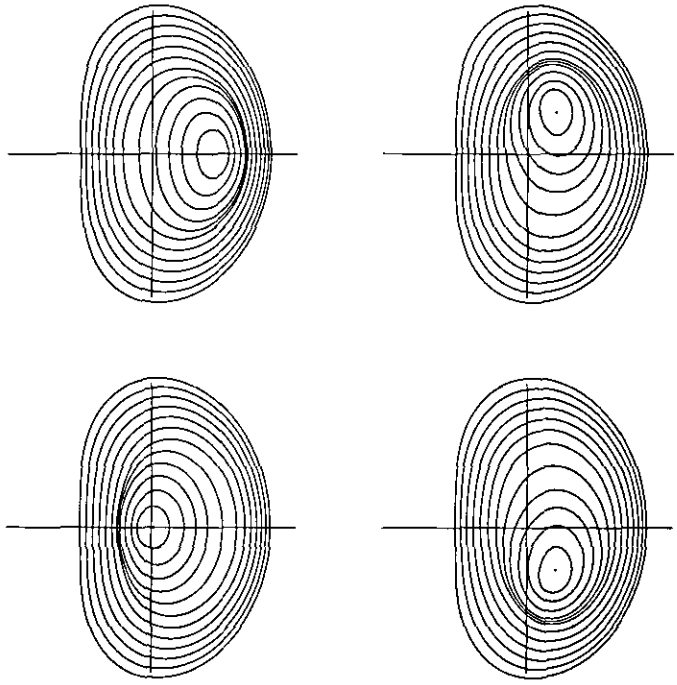

FIG. 4. An $m = 1$, $n = 1$ mode in the ITER tokamak with $\beta = 4.4\%$. A current sheet has developed where ι crosses unity, and it becomes clearly visible in this calculation on a $12 \times 12 \times 12$ mesh of radial, toroidal, and poloidal points and Fourier terms up to degree 4×4. This plot is evidence of the contention that the NSTAB code captures weak solutions of the equilibrium problem characterized by nested KAM surfaces.

energy landscape to determine stability. The bifurcated solutions do indeed have lower energy than the axisymmetric solution, but the difference is small, and convergence studies become difficult in the harder cases with more complicated geometry.

The bifurcated equilibria can be produced by simply using many iterations and allowing noise to trigger the unstable mode. When such a run is made, it at first converges to the axisymmetric solution. As the iteration proceeds, the energy decreases monotonically to the axisymmetric value, where it remains until the mode finally emerges. Then the energy starts to decrease further and the run converges to a bifurcated solution like the one shown in Fig. 4.

This procedure can be greatly acclerated by the use of an inhomogeneous term as described in [14]. At $t = 1$ we look for the internal kink mode which has an $m = 1$, $n = 1$ mode structure. To trigger this mode, we add an $m = 1$, $n = 1$ inhomogeneous term ξ to the partial differential equations for a few hundred iterations. We use a term for ξ similar to that given in the references about a second energy minimization [2, 3]. After the term has been removed the run converges to the bifurcated equilibrium shown in Fig. 4. The convergence rate for the bifurcated solution is substantially slower than the convergence rate of the axisymmetric solution. The axisymmetric case completely converges in 1000 iterations. While it only takes 3000 iterations to establish the existence of a bifurcated solution, 50,000 iterations are required to converge the run to 14 significant figures in the energy, which takes 15 min on the CRAY Y-MP computer.

7. STABILITY TEST

In addition to the localized current sheet modes in the previous example, our computational method also has the resolution to test for nonlinear instability by looking for bifurcated solutions with broader perturbations. Such computations require many poloidal and toroidal harmonics because the instabilities are associated with high mode numbers.

One example is the LHD stellarator described in Section 5. In the standard configuration it is known to be marginally stable [12]. However, we analyze a family of nearby configurations that can be made unstable by reducing the outward shift of the magnetic axis. This is achieved by adding small harmonics to the shape of the outer wall that model the effect of increasing the vertical magnetic field. For moderate shifts, bifurcated solutions appear over two field periods of the device. The existence of these additional solutions prove that the more standard equilibria for these nearby configurations (obtained by performing the calculations in just one field period) are unstable.

A ballooning instability is shown in the bifurcated equilibrium presented in Fig. 5. This calculation was performed in two field periods, with an average β of 3%. Small values $\Delta_{1,1} = 0.03$ and $\Delta_{3,1} = 0.01$ were added to the shape of the outer wall, but they are barely visible in the figure. They have the effect of reducing the outward shift of the magnetic axis from 28% to 22% of the plasma radius. The mode appears in the middle third of the plasma volume, where the rotational transform crosses $\frac{5}{6}$ and $\frac{5}{5}$, so it has a combined $m = 6$, $n = 5$ and $m = 5$, $n = 5$ structure over the full 10 field periods of the LHD.

This bifurcated solution is computed in a similar manner as the current sheet mode in the tokamak. The calculations are performed in two field periods, where the mode has an $m = 6$, $n = 1$ and $m = 5$, $n = 1$ structure. The mode is triggered by the temporary addition of an $m = 6$, $n = 1$ inhomogeneous term to the equilibrium equations. After this term is released the mode decays quickly, but it eventually levels off to a value which produced the bifurcated solution shown in Fig. 5. The computation required 3000 iterations and used 30 min of CPU time on the CRAY Y-MP to converge to seven significant figures in the energy. It was performed with 22 radial points and a trigonometric polynomial of degree $N_u = 16$ in the poloidal angle and $N_v = 24$ in the toroidal angle.

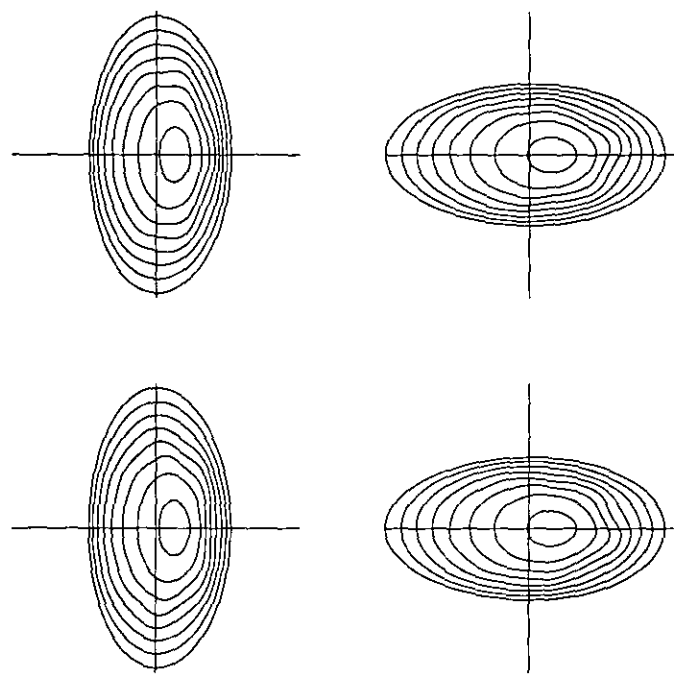

FIG. 5. *Four cross sections of two field periods of a bifurcated LHD* stellarator equilibrium with $\beta = 3\%$ are shown. A mode which breaks the one field period symmetry is visible. In two field periods, the mode has an $m = 6$, $n = 1$ and $m = 5$, $n = 1$ structure. Small sidebands $\Delta_{1,1} = 0.03$ and $\Delta_{3,1} = 0.01$ in the shape of the separatrix have reduced the usual outward shift of the magnetic axis, destabilizing what is otherwise considered to be a standard configuration. Nonuniqueness of the solution is made evident by the asymmetry.

It is important to choose a fine enough mesh if instabilities are to be resolved. For the mode described above, meshes with as few as 15 radial points are adequate. However, in the poloidal direction harmonics must be allowed up to $N_u = 16$. If less are used, the mode is not seen because one must resolve adequately its $m = 7$ sideband and $m = 12$ overtone.

It is only in special cases that we can compute completely converged bifurcated equilibria. For example, in stable configurations of the LHD with smaller values of the sidebands in the outer wall, the mode decays after the inhomogeneous term is removed, eventually becoming negligible. On the other hand, if the value of $\Delta_{3,1}$ is increased to 0.02 moving the axis in another 5%, the equilibrium becomes highly unstable. After the inhomogeneous term is removed the mode grows so large that the computations eventually break down. In such cases the energy decreases indefinitely and is clearly lower than the energy of the regular equilibrium. The difference of the energy levels in this case is in the seventh figure.

The method seems well adapted to modes associated with rational surfaces corresponding to moderate m and n values which occur in one or two field periods. To determine if a configuration is stable with respect to this type of mode, one must attempt to trigger all such modes. A range of design parameters must also be studied to determine if a reasonably sized stable regime exists and to validate the technique by showing that there are also regimes where instabilities are detected. Lower modes, such as the $m = 2$, $n = 1$, occur in the full 10 field periods of the LHD, where the calculations are more difficult for this technique due to the different length scales involved.

Stellarators may also have very poor plasma confinement for reasons not associated with MHD instabilities. Using Monte Carlo methods to track individual particles in an LHD equilibrium provides a good estimate of transport [4, 5]. In the LHD, calculations based on a plasma radius of 60 cm, a magnetic field of $B = 4$ T, an average temperature of 3 keV, and a plasma density of 10^{14} cm^{-3} predict an energy confinement time of only 5 ms.

8. ADVANCED STELLARATORS

Compared to the tokamak and the LHD, many of the recently designed stellarators have a quite complicated shape. More harmonics are needed to represent the outer wall, and the solutions have a much fuller Fourier series. The fine structure of these devices and the large poloidal and toroidal meshes required to model them have caused difficulties with the equilibrium codes. We have developed a very robust, general tuning of the input parameters for NSTAB that works well in a variety of these harder cases.

Two advanced stellarators are presented here. The first is similar to the Helias designed in Germany [6], but has been modified to provide an unstable test case for the NSTAB code. We have calculated two different, fully converged bifurcated solutions over one field period of the device. The two dramatically deformed equilibria, shown in Figs. 6 and 7, were calculated by triggering the $m = 7$, $n = 6$ mode with opposite signs of the inhomogeneous term. The existence of these two minima leads us to conjecture that there is a third, less deformed but linearly unstable solution lying between these two bifurcated solutions. This is plausible because of the mountain pass theorem.

To capture this high order instability, the computations were performed with $N_u = 16$ and $N_v = 12$ which required 42 collocation points in the toroidal direction and 36 in the poloidal direction. The mode is not seen if less harmonics are used, but just 19 radial points were sufficient. One of these cases has been run for 40,000 iterations, taking 200 minutes on the CRAY Y-MP and convergence of the bifurcated solutions to nine significant figures in the energy was observed. The computed rotational transform varies between $\frac{6}{7}$ and $\frac{6}{8}$ with very little shear, and the stellarator has an aspect ratio of 10 with six field periods and a pressure profile $p(s) = 0.03(1 - s)$ at $\beta = 3\%$.

Our second case is a model of the H1 Heliac at the Australian National University. This experiment has a large

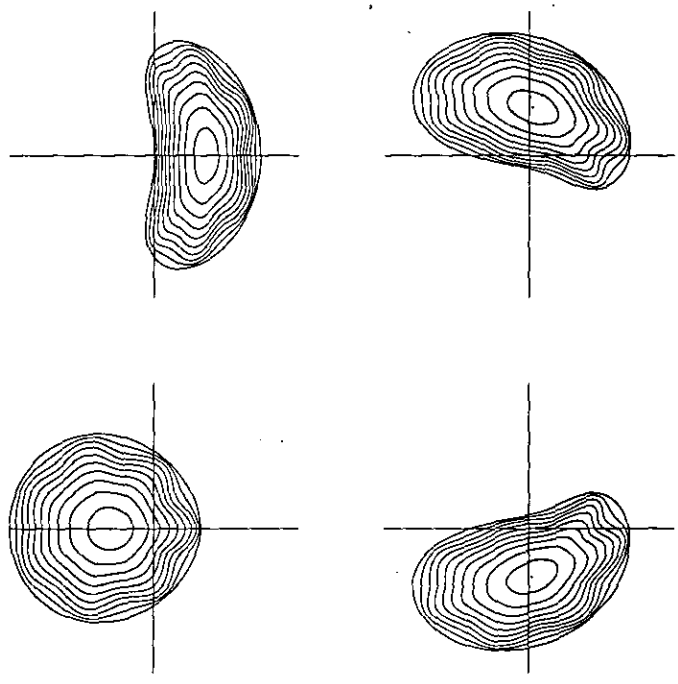

FIG. 6. Four cross sections of one field period of a bifurcated equilibrium soution for an advanced stellarator configuration with $\beta = 3\%$. In one field period, ι is roughly $\frac{1}{7}$ throughout the plasma, and the mode clearly shows an $m = 7$, $n = 1$ structure. The run has exemplary convergence, establishing that the NSTAB code can handle equilibria with complicated harmonics on a fine mesh with $22 \times 48 \times 36$ points and Fourier terms up to degree 16×12.

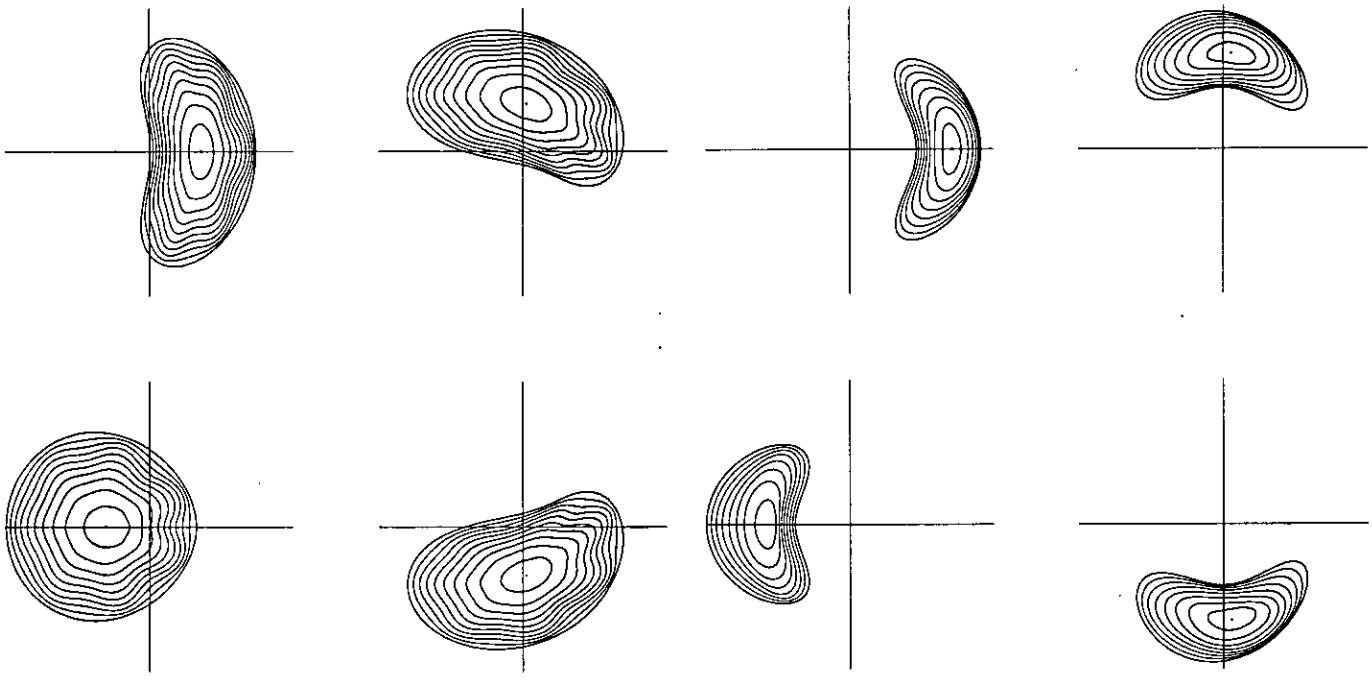

FIG. 7. A bifurcated equilibrium for the advanced stellarator similar to that shown in Fig. 6 but with the opposite sign of the displacement, which establishes the existence of two different solutions.

FIG. 8. Four cross sections of one field period of the $\beta = 2\%$ H1 Heliac at ANU. The complicated triangularity and crescent structure of this case were resolved on a mesh with $15 \times 36 \times 36$ points and Fourier terms up to degree 12×12. The run has converged to 11 significant figures in the energy.

helical excursion of the magnetic axis and pronounced triangularity of the wall shape, so many harmonics are required to describe the solution. We used an aspect ratio $A = 5$, three field periods and a pressure profile $p(s) = 0.055(1-s)^2$ which gives $\beta = 2\%$. The plasma wall is defined by $\Delta_{1,1} = 1.25$, $\Delta_{-1,-1} = 0.30$, $\Delta_{2,1} = -0.10$, $\Delta_{2,2} = -0.36$, and $\Delta_{3,3} = 0.10$.

A fully converged equilibrium computed by the NSTAB code is shown in Fig. 8. The computed rotational transform increases from 1.08 on axis to 1.14 at the outer wall. For this run we used 15 radial points and degree $N_u = N_v = 12$ for the trigonometric polynomials. Rezoning of the outer wall to distribute the collocation points well on the inner flux surfaces proved important in achieving good convergence. It was rezoned in u (see Section 4) by setting $Z_{-1,-1} = 0.30$, $Z_{2,1} = -0.10$, $Z_{2,2} = -0.15$, $Z_{3,3} = 0.10$, and making the change of variable $u' = u - v$. In a series of runs at the Australian National University it was not possible to get the VMEC code to converge on such a fine mesh. We have also been unable to get BETAS to converge in this case, although the performance of both codes could probably be improved with additional tuning.

The H1 equilibrium computed by NSTAB required 2 h on a CRAY 2 and 40,000 iterations to achieve 11 significant figures in the energy, and there is no reason to believe that NSTAB would not converge to more figures if the run were continued. The energy E reached a minimum when only nine of the 11 figures had stabilized, and then E was increasing as it converged to its final value. In using the spectral method, this type of behavior is not unexpected, since the discrete quadrature formula for the energy is not directly related to the discrete equilibrium equations as it would be if finite differences or finite elements were used.

9. CONCLUSIONS

We have developed the new three-dimensional MHD equilibrium code NSTAB. The code uses the spectral method and a flux coordinate formulation of the variational principle associated with the MHD equations. It has the resolution to compute bifurcated equilibria with well-resolved current sheets at rational surfaces and other, broader perturbations. A configuration is considered to be nonlinearly unstable when several bifurcated solutions can be shown to exist. It is less practical to use the energy landscape to determine stability properties, although in cases where comparisons are possible the energy levels of the bifurcated solutions are less than those of the more standard equilibria, verifying that they represent true physical instabilities.

The method has low order convergence with respect to the radial mesh size, but is still highly accurate. Conclusive stability tests can be performed with as few as 15 radial mesh points. The method is well adapted to the moderate

mode numbers of the instabilities that develop in one or two field periods of typical stellarators. To capture bifurcated solutions with these modes, many poloidal and toroidal harmonics must be used, but NSTAB does converge in these hard cases.

We have given a new residue condition to determine the location of the magnetic axis. It is derived from the weak form of the equations resulting from the variational principle and imposes no constraints on the shape of the flux surfaces. Several simplifications are made to implement the condition numerically, but it has held up well in practice. In cases with elliptical flux surfaces at the axis the resulting condition is related to the geometrical condition used by BETAS and there is good agreement between NSTAB and BETAS. In harder cases, the lack of constraints allows for more realistic flux surfaces. The shape of these surfaces can have a significant effect on the axis location, which is critical for accurate stability results.

ACKNOWLEDGMENTS

I would like to thank my thesis advisor, Paul Garabedian, for his support of this work and for all that he has taught me. I would also like to thank Frances Bauer and Michael Tippett for many useful discussions. Henry Gardner has kindly given us access to his runs of the VMEC code at the Australian National University. This work was supported by U.S. Department of Energy Grants DE-FG02-86ER53223 and DE-FG02-93ER25160, National Science Foundation Grant DMS-8922805, the National Science Foundation Graduate Fellowship Program, and the Pittsburgh Supercomputing Center.

REFERENCES

1. F. Bauer, O. Betancourt, and P. R. Garabedian, *A Computational Method in Plasma Physics* (Springer-Verlag, New York, 1978).
2. F. Bauer, O. Betancourt, and P. R. Garabedian, *Magnetohydrodynamic Equilibrium and Stability of Stellarators* (Springer-Verlag, New York, 1984).
3. F. Bauer, O. Betancourt, P. R. Garabedian, and M. Wakatani, *The Beta Equilibrium, Stability, and Transport Codes* (Academic Press, London, 1987).
4. P. R. Garabedian and M. Taylor, *Commun. Pure Appl. Math.* **44**, 1000 (1991).
5. P. R. Garabedian and M. Taylor, *Nucl. Fusion* **32**, 265 (1992).
6. J. Nührenberg and R. Zille, *Phys. Lett. A* **114**, 129 (1986).
7. S. P. Hirshman and J. T. Hogan, *J. Comput. Phys.* **63**, 329 (1986).
8. S. P. Hirshman, U. Schwenn, and J. Nührenberg, *J. Comput. Phys.* **87**, 396 (1990).
9. O. Betancourt, *Commun. Pure Appl. Math.* **41**, 551 (1988).
10. S. P. Hirshman and O. Betancourt, *J. Comput. Phys.* **96**, 99 (1991).
11. D. V. Anderson, W. Cooper, R. Gruber, S. Merazzi, and U. Schwenn, *Int. J. Supercomput. Appl.* **4**, 34 (1990).
12. Y. Nakamura, K. Ichiguchi, M. Wakatani, and J. L. Johnson, *J. Phys. Soc. Japan* **9**, 3157 (1989).
13. S. Frankel, *Math. Tables Aids Comput.* **4**, 65 (1950).
14. M. Taylor, Ph.D. thesis, New York University, October 1992.
15. D. Gottlieb and S. A. Orszag, *Numerical Analysis of Spectral Methods* (Soc. Indus. Appl. Math., Philadelphia, 1977).
16. S. P. Hirshman and H. Weitzner, *Phys. Fluids* **28**, 1207 (1985).
17. J. G. Cordey, R. J. Goldston, and R. R. Parker, *Phys. Today* **45**, 22 (1992).